Chemosphere 307 (2022) 135991

Contents lists available at ScienceDirect

Chemosphere

journal homepage: www.elsevier.com/locate/chemosphere

Shedding light on the performance of magnetically recoverable TiO_2/Fe_3O_4/rGO-5 photocatalyst. Degradation of S-metolachlor as case study

Carmen Barquín, María J. Rivero, Inmaculada Ortiz *

Departamento de Ingenierías Química y Biomolecular, Universidad de Cantabria, Avda. Los Castros, s/n, 39005, Santander, Spain

HIGHLIGHTS

- TiO_2/Fe_3O_4/rGO-5 photocatalysts synthesised via sustainable hydrothermal method.
- S-metolachlor photocatalytic degradation with TiO_2, TiO_2/rGO-5 and TiO_2/Fe_3O_4/rGO-5.
- Reduced graphene oxide enhances electronic conductivity and photocatalytic activity.
- Magnetic properties of TiO_2/Fe_3O_4/rGO-5 favours recovery and reuse.
- Scavenger test proved hydroxyl radicals are the predominant reactive oxygen specie.

GRAPHICAL ABSTRACT

Graphical abstract. Proposed graphical mechanism for each photocatalyst.

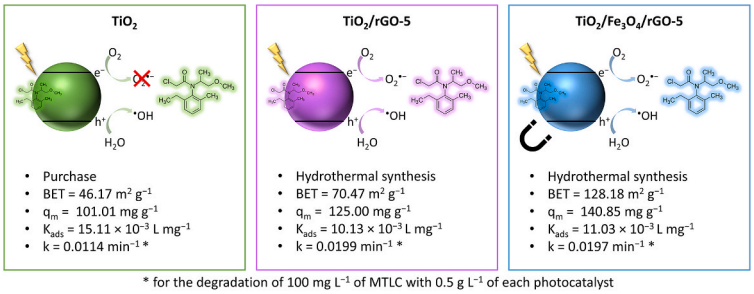

* for the degradation of 100 mg L^{-1} of MTLC with 0.5 g L^{-1} of each photocatalyst

ARTICLE INFO

Handling Editor: Sergi Garcia-Segura

Keywords:
Photocatalysts
TiO_2/Fe_3O_4/rGO-5
S-metolachlor
Reusability
Reactive oxygen species

ABSTRACT

Recalcitrant contaminants are not usually removed in conventional wastewater treatment plants. Therefore, they are transferred to the water resources that receive treated wastewaters and their presence can cause health and environmental issues. Herbicides are among these compounds. In particular, S-metolachlor (MTLC) is specifically of high concern because its molecule incorporates a chlorine atom that contributes to its toxicity. For its removal, a magnetically recoverable photocatalyst, TiO_2/Fe_3O_4/rGO-5, was synthesised following a hydrothermal method. The performance of TiO_2/Fe_3O_4/rGO-5 has been experimentally assessed and compared to TiO_2 and TiO_2/rGO-5 catalysts. A characterisation of the materials properties was carried out including adsorption isotherms of MTLC that provided the maximum adsorption capacity of the materials (q_m), being 140.85 ± 5.14 mg g^{-1} for TiO_2/Fe_3O_4/rGO-5. Furthermore, the ternary composite exhibited good recoverability from liquid media after four consecutive cycles thanks to its magnetic character (magnetic saturation of 13.85 emu g^{-1}). Photocatalytic degradation of MTLC started after a dark adsorption step following first order kinetics (0.0197 ± 1.2 × 10^{-4} min^{-1} for the degradation of 100 mg L^{-1} of MTLC with 0.5 g L^{-1} of TiO_2/Fe_3O_4/rGO-5) similar to the rate of appearance of chloride in solution; after total removal of the solubilized MTLC the chloride concentration in the solution continued increasing with zero-th order kinetics up to the value corresponding to the total MTLC concentration. This second step in the chloride formation was attributed to the degradation of adsorbed MTLC. Specific experiments in the presence of scavengers of reactive oxygen species (ROS) were carried out shedding light on the degradation mechanisms. It was concluded the predominant role of free hydroxyl radicals in the photocatalytic degradation in all the investigated materials, whereas the presence of rGO in the composite photocatalysts improved their electronic conductivity, enhancing the activity of superoxide radicals. The results of this work provide important information for further development of photocatalysis.

* Corresponding author.
E-mail address: ortizi@unican.es (I. Ortiz).

https://doi.org/10.1016/j.chemosphere.2022.135991
Received 22 April 2022; Received in revised form 11 July 2022; Accepted 7 August 2022
Available online 10 August 2022

1. Introduction

The increase in world population implies the corresponding increase in the demand for food crops and water consumption. Currently, 70% of the world's freshwater withdrawal is used for agriculture. This, together with the extended use of phytosanitary products, herbicides and pesticides, contributes to the deterioration of the quality of runoff receiving water resources and soils (Hotloś, 2008). Among herbicides, S-metolachlor (MTLC), $C_{15}H_{22}ClNO_2$, is widely used in broad-leaf weed control (Klein et al., 2006; Sakkas et al., 2004), implying difficult biodegradation and toxicity, as it has a chlorine atom (Zemolin et al., 2014). Concentrations in surface and ground water have been detected from 0.1 to 10 μg L^{-1} (Orge et al., 2017) and MTLC appears in the Drinking Water Contaminant Candidate List of the USEPA (USEPA, 2022).

Whether for discharge or to be reused, economically viable and efficient alternatives are necessary for water remediation, in the framework of the sustainable development goal number 6, Clean Water and Sanitation. Heterogeneous photocatalysis is an adequate technology both for hydrogen generation and for the removal of recalcitrant organic compounds in aqueous matrices (Al-Mamun et al., 2019; Corredor et al., 2021; Gholami et al., 2020; Liu et al., 2021a, 2021b; Nguyen et al., 2020; Tayyab et al., 2022; Varma et al., 2020; Wang et al., 2020). When the irradiation energy is higher to the band-gap of the semiconductor (SC), the electron-hole pairs are generated, being responsible of the formation of species involved in the oxidative and reductive reactions (Diban et al., 2021; Fernández-Castro et al., 2015; Koe et al., 2020; Nosaka and Nosaka, 2017; Padmanabhan et al., 2021).

TiO_2 is the most widely used photocatalyst but its particles diameter (≈ 25–35 nm) are difficult to recover, becoming a problem for practical engineering (Chen et al., 2020; Oppenländer, 2002). Reduced graphene oxide (rGO) is one promising alternative to combine with TiO_2 due to its capacity to enhance the electrons movement, improve the photocatalytic activity and reduce the electron-hole pair recombination (Balsamo et al., 2021; Corredor et al., 2020; Fogaça et al., 2021; Gupta and Melvin, 2017; Wanag et al., 2021). To enhance the photocatalyst separation from solution, magnetic oxides have received much attention because particles can be easily separated using a magnetic field (Karthikeyan et al., 2020). Magnetite (Fe_3O_4), in addition to its magnetic properties, can also prevent the aggregation and restacking of graphene sheets, providing a high surface area (Sun et al., 2011). Scientific community is focused on the adsorption capacity of magnetite-based materials for the removal of contaminants from aqueous matrices, including the efficient adsorption of SARS-CoV-2 spike pseudo-virus (Karimi-Maleh et al., 2020; Maimaiti et al., 2022; Minitha et al., 2018; Zhou et al., 2022). Special emphasis on the search for efficient and reusable materials, such as TiO_2/Fe_3O_4/rGO, which combine the good properties of each individual compound and is able to enhance photocatalytic activity (Benjwal et al., 2015; Bibi et al., 2021; Boruah and Das, 2020; Cheng et al., 2016; Fan et al., 2021; Li et al., 2015). Table S1 in the supplementary material includes details of literature works related to the same type of catalyst.

The novelty of this work lies on the study of the degradation of contaminants of emerging concern from aqueous matrices, S-metolachlor in particular, while using the heterogeneous photocatalysis as efficient technology. For that purpose, a ternary photocatalyst made of TiO_2, Fe_3O_4 and rGO, TiO_2/Fe_3O_4/rGO-5, with a composition of 47.5/47.5/5% wt. respectively, was synthesised. A detailed study of the adsorption stage has also been carried out. For testing TiO_2/Fe_3O_4/rGO-5, a comparative photocatalytic study was performed using TiO_2 and TiO_2/rGO-5 (95/5% wt. respectively). Catalyst reusability has been tested due to the magnetic character of TiO_2/Fe_3O_4/rGO-5. Finally, different photocatalytic mechanisms for each catalyst were proposed, based on an exhaustive study of scavengers that inhibit specific reactive oxygen species (ROS) involved in the processes.

2. Methodology

2.1. Materials

S-metolachlor (MTLC) PESTANAL®, iron(III) chloride ($FeCl_3$), acetonitrile LiChrosolv® and *p*-benzoquinone (BQ) were purchased from Sigma-Aldrich. Iron(II) chloride tetrahydrate ($FeCl_2{\cdot}4H_2O$) 99+% and *tert*-butyl alcohol (t-BuOH) 99.5% were supplied by Acros Organics. Titanium dioxide (TiO_2) Aeroxide® P25 was provided by Evonik Degussa. Graphene oxide (GO) water dispersion 4 mg mL^{-1} was acquired from Graphenea. Formic acid (FA) 85% from Panreac was used. Hydrochloric acid (HCl) 0.1 M and sodium hydroxide (NaOH) EMSURE® solution 50% were employed when necessary pH control, from Fisher Chemical and Merck, respectively. All reagents and materials were analytically pure and employed without further treatment.

2.2. Preparation of composites

The binary and ternary composites, TiO_2/rGO-5 and TiO_2/Fe_3O_4/rGO-5, were prepared following the procedures described in the supplementary material.

2.3. Photocatalysts characterisation

Morphological characterisation and elemental analysis were obtained by scanning electron microscopy (SEM) and energy dispersive analysis (EDX) using Carl Zeiss, model EVO MA15 microscope. Surface area was calculated from N_2 adsorption-desorption isotherms at 77 K measured in an ASAP 2420 Micromeritics. Fourier transform infrared (FTIR) spectra were recorded in a Perkin Elmer equipment, model Spectrum Two. Raman spectra were recorded by Confocal-Raman NRS-4500 JASCO using a green diode laser excitation source (531.90 nm). X-ray diffraction spectra (XRD) were obtained in a Bruker D8 Advance instrument fitted with a Cu tube with a wavelength of 0.15418 nm, the spectrum was collected at 2Θ angles between 5 and 80 °. Zeta potential of the photocatalysts was measured in a Zetasizer Nano ZS from Malvern at pH range 2.5–12. X-ray photoelectron spectroscopy (XPS) measurements were performed using a SPECS Phoibos 100 system with Al kα radiation (1486.6 eV) obtained from a monochromatic source applying 14.00 kV and 175 W. Magnetic properties of the magnetic samples were investigated with a Quantum Design MPMS XL-5 SQUID magnetometer whilst heating from 2 to 300 K under different applied magnetic fields from 1 to 85 kOe. Electrochemical measurements were conducted via cyclic voltammetry in an aqueous solution with a DRP-250AT gold electrode. Voltammograms were recorder as the potential was swept at a scan rate of 0.1 V s^{-1}.

2.4. Adsorption isotherms

MTLC adsorption isotherms were determined in batch adsorption experiments at room temperature in the dark. 100 mL of aqueous solution containing different catalyst loads (0.50, 0.75 and 1.00 g L^{-1}) and also different initial MTLC concentrations (30, 100 and 200 mg L^{-1}) were studied employing Erlenmeyer flasks. Samples were shaken for 1 h at 500 rpm, proving that in this period of time the adsorption-desorption equilibrium was reached. The adsorbed capacity was calculated according to equation (1):

$$q_e = ((C_0 - C_e)V) / M \quad (1)$$

where q_e is the equilibrium adsorption capacity of the adsorbent (mg g^{-1}), C_0 is the initial MTLC concentration (mg L^{-1}), C_e is the equilibrium concentration of MTLC (mg L^{-1}), V is the solution volume (L) and M is the adsorbent mass (g).

2.5. Photocatalytic activity

The photocatalytic activities were evaluated for the removal of synthetic MTLC solutions in aqueous phase. Experiments were performed in a 1 L Pyrex glass photoreactor provided with UV-A LED technology from APRIA SYSTEMS. The reactor housing had 30 LEDs (ENGIN LZ1-00UV00) distributed in 10 strips, placed at a distance of 1.50 cm from the photoreactor. After the adsorption period, the suspension was irradiated with an average of 200 W m^{-2}. Samples were collected, filtered through a nylon syringe filter (0.45 μm, FILTER-LAB®) and analysed afterwards. Two initial MTLC concentrations were studied: 30 and 100 mg L^{-1}, equivalent to 0.11 and 0.35 mM respectively, with also two different catalyst loads: 0.5 and 1.0 g L^{-1}.

MTLC concentration was quantified in a high-performance liquid chromatograph (HPLC) from Agilent, Series 1100, equipped with an Agilent Zorbax 80 Å Extend-C18 column (5 μm, 3.0 × 150 mm) coupled to a diode array detector (1260 DAD-HS). Ultrapure water and acetonitrile were the mobile phases in a ratio 40/60, a flow rate of 0.70 mL min^{-1} and 50 μL as injection volume. The retention time was 3.8 min. The selected wavelength was 214 nm. The column temperature was kept at 30 °C. The total organic carbon (TOC), used to quantify the mineralisation degree, was measured in a Shimadzu TOC-V-CPH analyser provided with autosampler. The released chloride to the solution was determined in an ion chromatograph with autosampler, Dionex ICS-5000 using Na_2CO_3 9 mM as mobile phase with an anionic column IonPac AS9-HC (4.0 × 50 mm) from Thermo Scientific and a flow rate of 1.0 mL min^{-1}. For the analysis of ROS, BQ, t-BuOH and FA were used as scavengers, whose concentrations were set based on the results reported in a previous publication (Ribao et al., 2019). When needed, pH was monitored with a Hanna pHmeter, model edge.

3. Results and discussion

3.1. Photocatalysts characterisation

Surface morphology and particle size of the photocatalysts were elucidated by scanning electron microscopy (SEM) analysis. Fig. 1a–c represents the SEM micrographs of fresh TiO_2, TiO_2/rGO-5 and TiO_2/Fe_3O_4/rGO-5, respectively. The quasi-spherical morphology of TiO_2 particles with sizes bellow 5 μm, which are relatively bigger in size than the average particle diameter reported in literature for P25, is observed in Fig. 1a. This difference is attributed to the TiO_2 agglomeration. For TiO_2/rGO-5, Fig. 1b, the particles were bigger compared to TiO_2 and they had irregular shapes with diameters in the order of 50 μm. Regarding TiO_2/Fe_3O_4/rGO-5, Fig. 1c, irregular particles and sizes slightly higher than TiO_2/rGO-5 were observed. Fig. 1d shows the TiO_2/Fe_3O_4/rGO-5 particles after being used in 4 consecutive photocatalytic experiments, TiO_2/Fe_3O_4/rGO-5 (R3), assessing the catalyst stability. The particles diameter slightly decreases after use probably due to the constant stirring.

Elemental analysis of each photocatalyst using EDX spectra is presented in Table S2 in the supplementary material. Table S3 shows the BET and BJH results of the materials. TiO_2, TiO_2/rGO-5 and TiO_2/Fe_3O_4/rGO-5 have a BET surface area of 46.17, 70.47 and 128.18 m^2 g^{-1}, respectively. Nitrogen adsorption isotherms for the three photocatalysts are shown in Fig. S1 in the supplementary material.

The surface properties of the materials can change with the pH of the solutions, influencing the photocatalytic activity. To this end, zeta potential of the materials was measured in the pH range 2.5–12, Fig. 2. GO was negatively charged on its surface regardless the pH, with values between −46 mV and −69 mV; the addition of GO to the materials will be reflected in a decrease of zeta potential values. For pH < 6, all materials except GO, were observed in the positively charged surface. Otherwise, at basic pH, the negatively charged surface of the materials was observed as illustrated in Fig. 2. Zeta potential of Fe_3O_4 was found to be +39 mV at pH 2.5 and it decreased down to −43 mV at pH 12. The isoelectric point (IEP) was obtained at pH ≈ 8. Meanwhile, IEP for TiO_2/rGO-5 composite was obtained at pH ≈ 5.8, which was slightly lower than IEP of TiO_2 (pH ≈ 6.3) due to the presence of rGO sheets. TiO_2 and TiO_2/rGO-5 had similar behaviour in terms of zeta potential. The zeta potential of TiO_2/Fe_3O_4/rGO-5 varied from +39 mV at pH 2.5 to −50 mV at pH 12, with an IEP value of ≈ 8.6, rather high as expected, with similar behaviour to Fe_3O_4.

Further characterisation is included in the supplementary material.

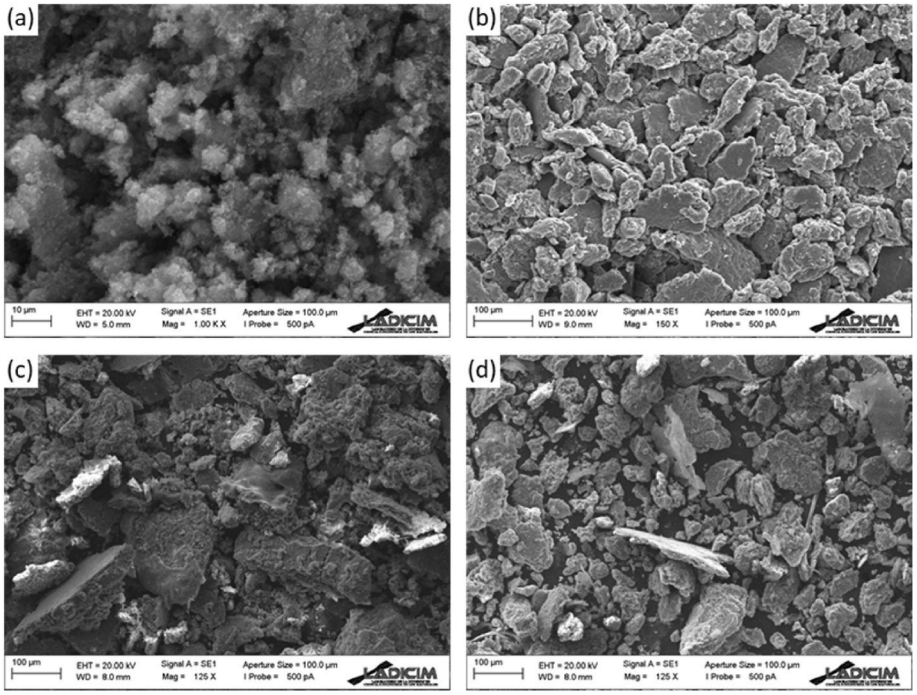

Fig. 1. SEM images of (a) TiO_2, (b) TiO_2/rGO-5, (c) TiO_2/Fe_3O_4/rGO-5 and (d) TiO_2/Fe_3O_4/rGO-5 (R3).

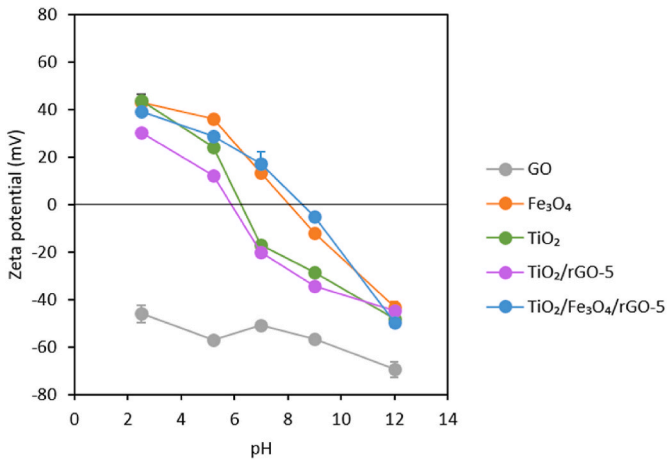

Fig. 2. Zeta potential of different materials.

3.2. Adsorption isotherms

Since many photocatalytic reactions are supposed to predominantly occur on the surface of the semiconductors (Bhatkhande et al., 2002), the adsorption of pollutants on the solid materials has been widely considered to play an important role in the photodegradation process. Fig. S9 shows the adsorption isotherms of MTLC on TiO_2, TiO_2/rGO-5 and TiO_2/Fe_3O_4/rGO-5. Langmuir isotherm, equation (2), was used to fit the experimental adsorption equilibrium data.

$$q_e = (q_m\, K_{ads}\, C_e) / (1 + K_{ads}\, C_e) \quad (2)$$

where q_e is the equilibrium concentration on the adsorbent (mg g^{-1}), q_m is the maximum adsorption capacity (mg g^{-1}), C_e is the equilibrium concentration of MTLC in the liquid solution (mg L^{-1}), and K_{ads} is the Langmuir's constant related to the energy of adsorption (L mg^{-1}). The Langmuir model considers the existence of a solute monolayer over the adsorbent surface, and it has been widely used to predict the adsorption behaviour in photocatalytic materials. The parameters of the fitting of the experimental results to the Langmuir model are listed in Table 1.

As represented in Fig. S9 and described in Table 1, the incorporation of rGO increased the adsorption capacity of TiO_2 by 25%, same increase that was observed in the BET specific surface area. Fe_3O_4 also increased the adsorption capacity of TiO_2/Fe_3O_4/rGO-5, in agreement to the BET area. TiO_2/Fe_3O_4/rGO-5 increased the adsorption capacity of TiO_2 by 40%, with a value of 140.85 ± 2.10 mg g^{-1}. During the synthesis of TiO_2/Fe_3O_4/rGO-5, the addition of iron oxides contributed to the reduction of GO and thus improved the hydrophobic character of the material; it is worth noting that hydrophobicity enhances MTLC adsorption. Moreover, the π electrons in the structure of rGO led to a facile π–π stack with the molecules that contained aromatic groups (Qin et al., 2014). In TiO_2/Fe_3O_4/rGO-5, the synergic interaction between Fe_3O_4 and TiO_2 could also enhance the adsorption capacity.

3.3. Photocatalytic activity

Photocatalytic degradation of MTLC with TiO_2, TiO_2/rGO-5 and TiO_2/Fe_3O_4/rGO-5 has been experimentally analysed under UV-A light irradiation. The analysis was carried out with 100 mg L^{-1} of MTLC using two different catalyst loads, 0.5 and 1.0 g L^{-1}. All experiments were kept in the dark for 1 h to ensure that the adsorption equilibrium had been reached. Afterwards, the light was turned on and the photocatalytic process started. Fig. 3 shows that in the absence of photocatalyst only a slight degradation of MTLC takes place.

Fig. 3a and b depicts MTLC elimination kinetics and the percentage of mineralisation after 330 min for 100 mg L^{-1} of MTLC and 0.5 g L^{-1} of catalyst. As it is observed, 21 ± 1.00, 31 ± 4.11 and 35 ± 3.10% of the initial MTLC was adsorbed on TiO_2, TiO_2/rGO-5 and TiO_2/Fe_3O_4/rGO-5, respectively, before the photocatalytic degradation. The composites enhanced the photocatalytic kinetics compared to TiO_2 leading to the values of the first order kinetic constants of 0.0114 ± 4.5 × 10^{-4}, 0.0199 ± 5.0 × 10^{-4} and 0.0197 ± 1.2 × 10^{-4} min^{-1} for TiO_2, TiO_2/rGO-5 and TiO_2/Fe_3O_4/rGO-5, respectively, Table 1.

Concerning mineralisation, Fig. 3b, binary composite provided the higher level of TOC elimination (51.77 ± 0.72% in 330 min of irradiation), followed by TiO_2/Fe_3O_4/rGO-5 (34.01 ± 1.32%) and TiO_2 (18.84 ± 2.30%).

The influence of the initial concentration was analysed in experiments with a MTLC concentration of 30 mg L^{-1} and 0.5 g L^{-1} of catalyst, Fig. S10a, for short and long operation times. It was observed the increase of the MTLC degradation rate with the decrease of the initial concentration. In terms of mineralisation, Fig. S10b, it is again observed the best performance of TiO_2/rGO-5, with a total TOC removal of 94.13 ± 0.60% after 480 min of irradiation. A similar trend but with a lower mineralisation degree, 77.30 ± 0.37%, was observed when using the ternary composite TiO_2/Fe_3O_4/rGO-5. Finally, traces of formic and acetic acid were detected in the last samples of all experiments, suggesting that the compounds that remain in the solution are short-chain and non-toxic organic molecules, as previously evidenced by Vieira Guelfi et al. (2018).

To evaluate the influence of the catalyst concentration, experiments with 1.00 g L^{-1} of each catalyst were carried out working with 100 mg L^{-1} of MTLC. Duplicating the catalyst loading, the adsorption capacity increased, Fig. 3c. The photocatalytic behaviour was slightly faster compared to the experiments with 0.5 g L^{-1} of each photocatalyst, as shown by the values of pseudo-first order kinetic constants reported in Table 1. The mineralisation percentage slightly increased, Fig. 3d, after 330 min of irradiation (between 4 and 15%) compared to the use of 0.5 g L^{-1} of each catalyst. Within this analysis, the good performance of the ternary TiO_2/Fe_3O_4/rGO-5 composite in the degradation of MTLC has been assessed.

Breakage of the MTLC molecule leads to the release of the chlorine atom of its molecule to the aqueous solution. Fig. 4 represents the dimensionless chloride concentration along the photocatalysis time of 30 and 100 mg L^{-1} of MTLC, respectively. Results of TiO_2/Fe_3O_4/rGO-5 are not shown because the remaining chloride in the synthesised catalyst (iron chloride) led to confusing results.

The results depicted in Fig. 4 show two different trends. First, when there is MTLC dissolved in the aqueous solution, the rate of MTLC

Table 1
Parameters of MTLC adsorption on the photocatalytic materials and first order degradation kinetics (100 mg L^{-1} of MTLC as initial concentration).

	Adsorption experiments			Photocatalytic experiments			
				100 mg L^{-1} MTLC, 0.5 g L^{-1} catalyst		100 mg L^{-1} MTLC, 1.0 g L^{-1} catalyst	
	q_m (mg g^{-1})	K_{ads} (L mg^{-1})	R^2	k (min^{-1})	R^2	k (min^{-1})	R^2
TiO_2	101.01 ± 2.54	15.11 × 10^{-3} ± 3.28 × 10^{-4}	0.98	0.0114 ± 4.5 × 10^{-4}	0.88	0.0166 ± 2.5 × 10^{-4}	0.97
TiO_2/rGO-5	125.00 ± 5.36	10.13 × 10^{-3} ± 3.35 × 10^{-4}	0.99	0.0199 ± 5.0 × 10^{-4}	0.96	0.0223 ± 5.2 × 10^{-4}	0.96
TiO_2/Fe_3O_4/rGO-5	140.85 ± 5.14	11.03 × 10^{-3} ± 2.38 × 10^{-4}	0.99	0.0197 ± 1.2 × 10^{-4}	0.94	0.0212 ± 4.5 × 10^{-4}	0.99

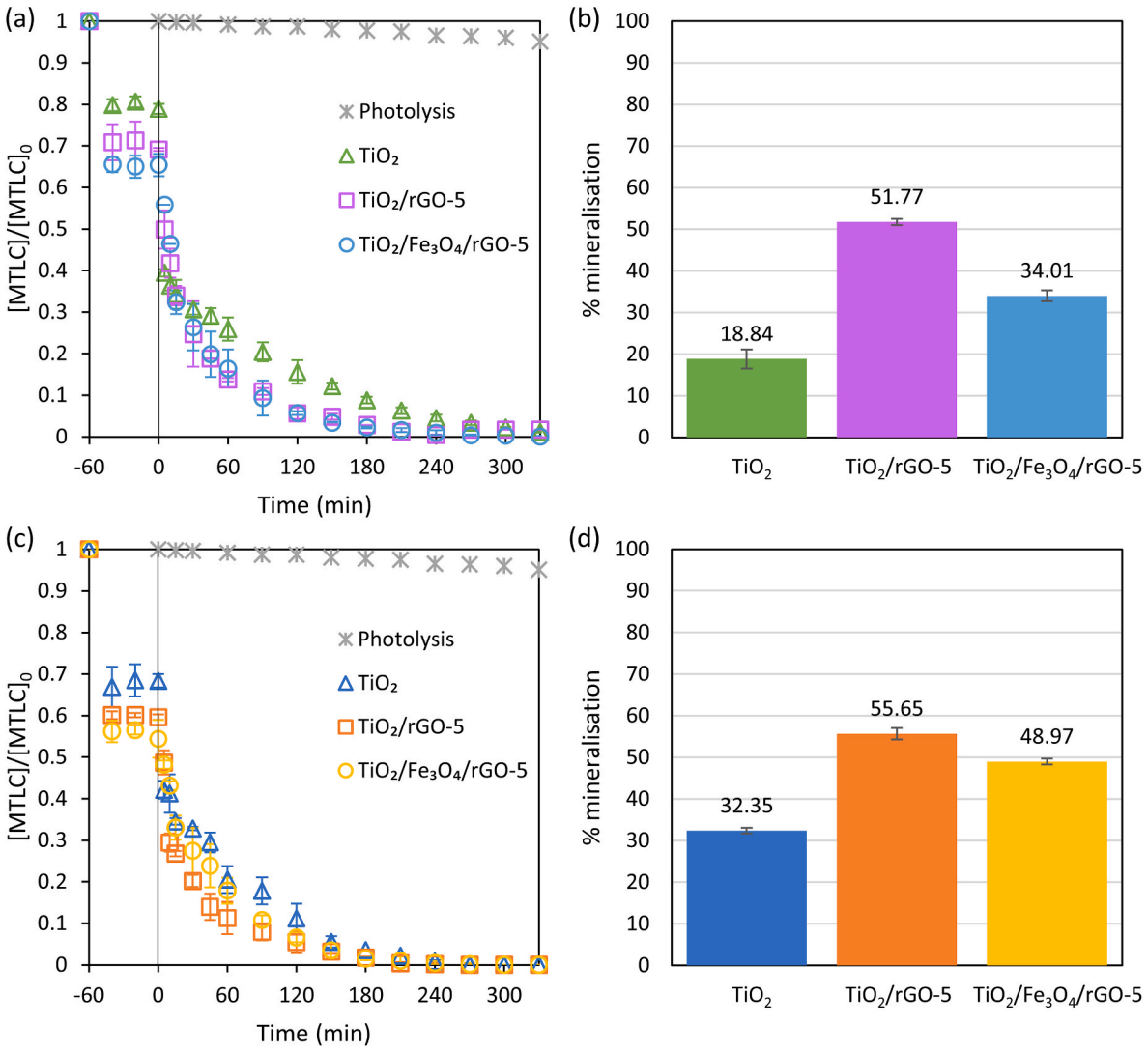

Fig. 3. MTLC removal and percentage of mineralisation after 330 min of irradiation with UV-A source at 365 nm. 100 mg L^{-1} of MTLC with 0.5 g L^{-1} (a), (b) and 1.0 g L^{-1} (c), (d) of catalyst in a total volume of 1 L.

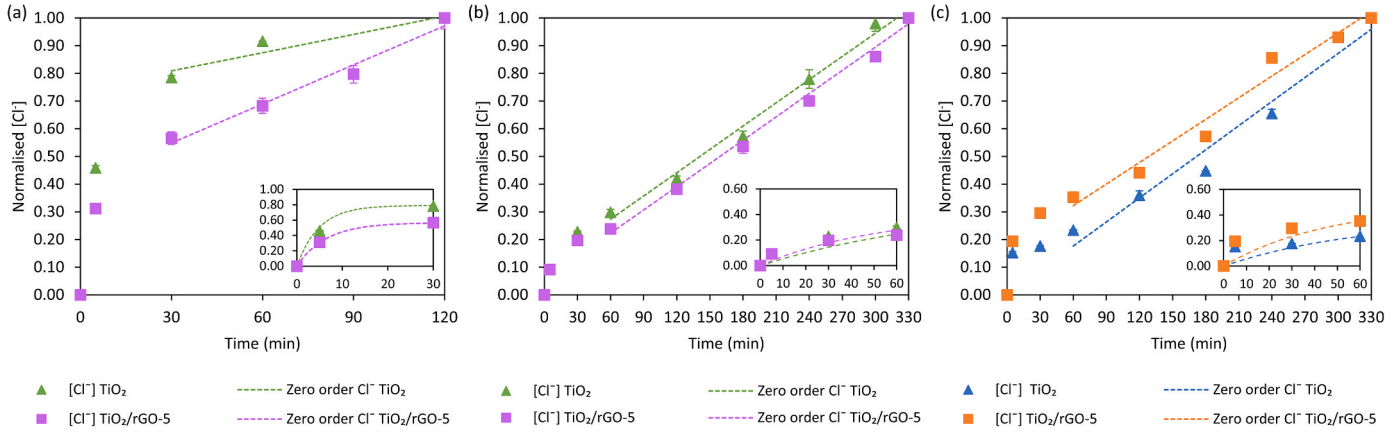

Fig. 4. Dimensionless chloride evolution in the solution for (a) 30 mg L^{-1} MTLC and 0.5 g L^{-1} catalyst, (b) 100 mg L^{-1} MTLC and 0.5 g L^{-1} catalyst and (c) 100 mg L^{-1} MTLC and 1.0 g L^{-1} catalyst and zero-th order fit. Inset: first order kinetics of chloride release.

degradation and chloride release fit to first order kinetics, insets of Fig. 4, with similar kinetic constants, Table 1. After the removal of the dissolved MTLC, the chloride concentration in solution kept increasing with time but a slower rate that was fitted to a zero-th order kinetics; parameters shown in Table S5. It is worth noting that the final chloride concentration in the solution matched the value of chlorine

concentration in the initial concentration of MTLC. Thus, it was hypothesized that this chloride could came from the adsorbed MTLC that would start its degradation after the complete disappearance of the soluble fraction. Furthermore, it can be also deduced that the intermediate organics formed after MTLC degradation are non-chlorinated organics as the chloride in solution closed the mass balance.

Separation and reusability of photocatalytic materials is still a challenge to be overcome for a wider deployment of the technology. Fig. 5 shows the yield of MTLC degradation in four consecutive cycles with the same ternary composite. After a photocatalytic experiment running for 120 min with 30 mg L^{-1} of MTLC and 0.5 g L^{-1} of TiO_2/Fe_3O_4/rGO-5, the photocatalyst was separated from the reaction medium with a neodymium magnet. Then, the material was dried in an oven at 80 °C for further use with freshly prepared MTLC solutions. Around 4% of the catalyst mass was lost in each experiment during the sampling procedure.

The efficiency of TiO_2/Fe_3O_4/rGO-5 composite for the removal of MTLC showed a drop lower than 10% after four cycles, which practically corresponds to the percentage of loss of catalyst mass in the sampling procedure. These results show the good catalyst recoverability.

3.4. Insight on the photocatalytic mechanism

Reduction and oxidation reactions take place simultaneously and ROS are produced sequentially from O_2 and H_2O. $^{\bullet}OH$, H_2O_2, $O_2^{\bullet-}$ and $^1O_2$ would be generated in this order by the stepwise oxidation of H_2O. Whereas, the stepwise reduction of O_2 generates $O_2^{\bullet-}$, H_2O_2 and $^{\bullet}OH$ (Nosaka and Nosaka, 2017). Further information about reactions that take place in the semiconductor can be found in the supplementary material as well as equations S1-S16.

To get insight on the mechanism of MTLC degradation, in this work several species that quickly react with radicals were employed. 1 g L^{-1} of BQ, 46.5 g L^{-1} of t-BuOH and 4.0 g L^{-1} of FA were used as scavengers, concentrations in excess regarding MTLC concentration (Ribao et al., 2019). BQ reacts with the electrons generated in the semiconductor, inhibiting principally the formation of $O_2^{\bullet-}$ (equation (3)). Further, although to a minor extent, BQ can partially react with $^{\bullet}OH$ and consequently impede their action on the degradation of MTLC (Cavalcante et al., 2016). Equation (4) shows the interaction between t-BuOH and $^{\bullet}OH_{free}$, inhibiting totally their effect. FA gets involved with h^+ and $^{\bullet}OH_{free}$, as expressed in equations (5) and (6); in this way, $^{\bullet}OH_{ads}$ are inhibited too.

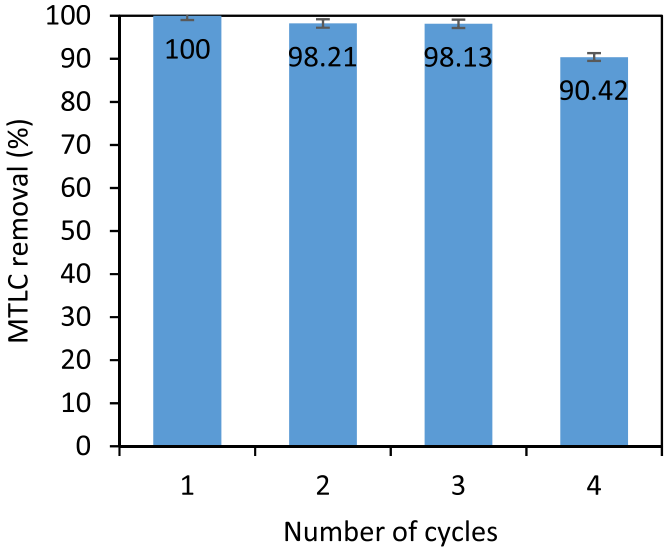

Fig. 5. TiO_2/Fe_3O_4/rGO-5 reusability studies under UV-A light irradiation (30 mg L^{-1} of MTLC and 0.5 g L^{-1} of catalyst).

$$O=C(C_2H_4)C=O+2e^-+2H^+\rightarrow HOC(C_4H_4)COH \quad (3)$$

$$(CH_3)_3COH+{}^{\bullet}O\,H_{free}\rightarrow\left(CH_2C(CH_3)_2OH\right)+H_2O \quad (4)$$

$$HCOO^-+2h^+\rightarrow CO_2+H^+ \quad (5)$$

$$HCOO^-+{}^{\bullet}O\,H_{free}\rightarrow CO_2^-+H_2O \quad (6)$$

The reaction rate constant between t-BuOH and $^{\bullet}OH$ is 5×10^8 M^{-1} s^{-1}, therefore, it would be a suitable $^{\bullet}OH$ scavenger (Bibi et al., 2021; Li et al., 2016; Ma and Graham, 2000). As detailed in equation (3), *p*-benzoquinone inhibits the formation of $O_2^{\bullet-}$ because it reacts with the electrons to form hydroquinone. Moreover, in the case that $O_2^{\bullet-}$ radicals have been formed, BQ will react fast with them due to the high kinetic constant of the reaction between BQ and $O_2^{\bullet-}$ ($0.9–1.0\times10^9$ M^{-1} s^{-1}) (Rodríguez et al., 2015). To determine the contribution of h^+ in the photocatalytic system, FA was used as scavenger. It can also inhibit the formation of $^{\bullet}OH_{free}$ because they react with the holes where they are produced (equation (4)) (Cavalcante et al., 2016). Therefore, electron-hole recombination is inhibited and the electrons could form $O_2^{\bullet-}$ (Pelaez et al., 2016).

The results of the MTLC photocatalytic degradation in the presence of scavengers and TiO_2, TiO_2/rGO-5 and TiO_2/Fe_3O_4/rGO-5 are shown in Fig. 5a–c, after the adsorption stage. Starting with TiO_2, it was evidenced the increase in the MTLC concentration after the addition of t-BuOH to the system. Li et al. (2016), Vital-Grappin et al. (2021) or Pelaez et al. (2016), have reported the tendency of t-BuOH to be adsorbed on the surface of the catalyst. As t-BuOH is in excess, it can be partially adsorbed while the rest remains in solution and reacts with the generated $^{\bullet}OH_{free}$. Thus, when the scavenger was added to the reaction solution, t-BuOH was adsorbed followed by a partial release of the adsorbed MTLC to the aqueous medium as there is a competition for the active sites of the catalyst. This adsorption phenomenon was tested with and without light irradiation (Fig. 5a), observing a similar behaviour. When light was turned on, $^{\bullet}OH$ are formed and they are quenched by t-BuOH, noticing that in the case of TiO_2, there is no MTLC degradation, because the MTLC concentration after adding t-BuOH keeps constant at the initial value. Therefore, by quenching the solution $^{\bullet}OH$, neither h^+ or $O_2^{\bullet-}$ are able to attack the organic molecule. In the presence of BQ, 17 ± 1.86% of MTLC disappears after 60 min of irradiation. BQ has also the ability to react with $^{\bullet}OH_{free}$ with a rate constant equal to 6.9×10^5 s^{-1} at pH 6.2 (Cavalcante et al., 2016). The lower the pH value the lower the value of the rate constant (Schuchmann et al., 1998). Thus, BQ could inhibit $O_2^{\bullet-}$ and $^{\bullet}OH$ at the same time, the latter at a slower rate than t-BuOH. In all the final samples of the experiments with BQ as scavenger, the presence of H_2O_2 was evidenced. In the absence of superoxide radicals, H_2O_2 could be formed through equations S11-S12. H_2O_2 can also lead to the indirect formation of $^{\bullet}OH$, equation S7, that may be responsible for the partial MTLC removal. A partial inhibition of the photo-oxidation process is observed when FA is added to the aqueous solution. 20 min of irradiation is the time corresponding to the total degradation of the solubilized MTLC in absence of scavengers, Fig. 5a. After adding FA, the solubilized MTLC concentration decreases by 28 ± 2.77%, in the first 20 min, reaching a minimum value at the time that the dissolved MTLC had disappeared completely in absence of scavengers. Afterwards, MTLC concentration starts increasing probably due to the partial desorption of the adsorbed solute until the S-L equilibrium is reached (Fujishima et al., 2008). This phenomenon could be possible because there are no ROS left in the system capable of further degrading MTLC. The partial degradation of MTLC in presence of FA could be due to the $^{\bullet}OH$ that react with MTLC before being quenched by FA, hypothesising that FA has lower capacity to quench $^{\bullet}OH$ than t-BuOH.

For TiO_2/rGO-5, Fig. 5b, MTLC concentration also experiments an increase after adding t-BuOH. Then, 10 ± 3.14% of MTLC disappeared after 60 min of photocatalysis even though $^{\bullet}OH$ were quenched. This could be attributed to the presence of $O_2^{\bullet-}$ and h^+. $O_2^{\bullet-}$ could be formed

following equation S3; probably promoted by the presence of rGO sheets that facilitate the electrons' movement and act as electron acceptors (Fogaça et al., 2021). With BQ, MTLC concentration decreases by 21 ± 2.67% after 60 min of irradiation. The degradation could be related with the indirect formation of $^{\bullet}OH$ from H_2O_2, equation S7, and also with h^+. In a system with TiO_2/rGO-5 and FA, MTLC concentration suffers a decrease during all the irradiation time, reaching a total decrease of 32 ± 0.12% after 60 min of UV-A. As previously explained, rGO is an excellent electron conductor, reason why $O_2^{\bullet-}$ could act facilely when TiO_2/rGO-5 photocatalyst is used and promote the MTLC degradation, showing the positive influence of the electronic conductivity. Moreover, $^{\bullet}OH$ also can also act in the system before being quenched by FA, but with a slower rate.

The scavenger analysis of t-BuOH for TiO_2/Fe_3O_4/rGO-5, Fig. 5c, follows a similar rationale to TiO_2/rGO-5. MTLC concentration increases after the addition of t-BuOH due to the adsorption of t-BuOH on the catalyst surface accompanied by MTLC desorption. Then, during the first 60 min of irradiation, there is a decrease of the MTLC concentration by 10 ± 2.17%, also attributed to the h^+ and to the presence of rGO sheets that are related with $O_2^{\bullet-}$ radicals. When BQ and FA are used, the behaviour with TiO_2/Fe_3O_4/rGO-5 is similar to TiO_2. With BQ, MTLC evidences a decrease of 14 ± 2.26% after 60 min of photocatalysis. As BQ inhibits the formation of $O_2^{\bullet-}$ and it can also react with $^{\bullet}OH$, H_2O_2 is formed through equations S11-S12. MTLC is degraded by the indirect formation of $^{\bullet}OH$ through equation S7 and also by h^+. Finally, in the presence of FA, MTLC concentration experiences a slight decrease of 14 ± 1.89% during the first 30 min of irradiation and then, MTLC is being desorbed until the S-L equilibrium is reached. Similar to TiO_2, during the initial 30 min of UV-A, MTLC disappears completely in absence of scavenger. Also, the presence of magnetite in the TiO_2/Fe_3O_4/rGO-5 composite worsens the action of rGO, which is likely to inhibit equations S6 and S15, reason why the behaviour of the ternary composite is more similar to TiO_2 than to TiO_2/rGO-5.

Overall, t-BuOH dramatically reduced the degradation rate of the photocatalytic MTLC degradation indicating that $^{\bullet}OH_{free}$ radicals are the predominant ROS responsible for the MTLC oxidation, above all in the case of TiO_2. TiO_2/rGO-5 and TiO_2/Fe_3O_4/rGO-5 took advantage of the electron conductivity of rGO sheets that contributed to enhance their performance and to observe the influence of $O_2^{\bullet-}$. All the above explanation is shown in Fig. 6d, where the proposed mechanism of the ternary catalyst in the degradation of MTLC is shown in graphical form.

4. Conclusions

A ternary composite, consisting of TiO_2, Fe_3O_4 and rGO has been synthesised following a facile and sustainable hydrothermal method. TiO_2/Fe_3O_4/rGO-5 showed an enhanced adsorption capacity compared to TiO_2 and TiO_2/rGO-5. MTLC degradation was evaluated under UV-A irradiation. After 210 min of irradiation, 100 mg L^{-1} of MTLC were completely removed from the solution with 0.5 g L^{-1} of TiO_2/Fe_3O_4/rGO-5 with a first order kinetic constant of 0.0197 ± 1.2 × 10^{-4} min^{-1}. Results confirm that with as-prepared composites TiO_2/rGO-5 and TiO_2/Fe_3O_4/rGO-5 it is possible to achieve a complete mineralisation of the aqueous solutions. All chlorine atoms from MTLC molecules are released as chlorides into the aqueous solution, first following first order kinetics, while MTLC in solution is degraded, and then with zero-th order kinetics, suggesting that the chloride in the second part comes from the degradation of the adsorbed MTLC. Due to its magnetic properties, TiO_2/Fe_3O_4/rGO-5 was reused in four consecutive runs with no significant differences in the MTLC removal yield. Specific experiments in presence of ROS scavengers proved that hydroxyl radicals are the main ROS acting with the three photocatalysts. Then, with TiO_2/rGO-5 and

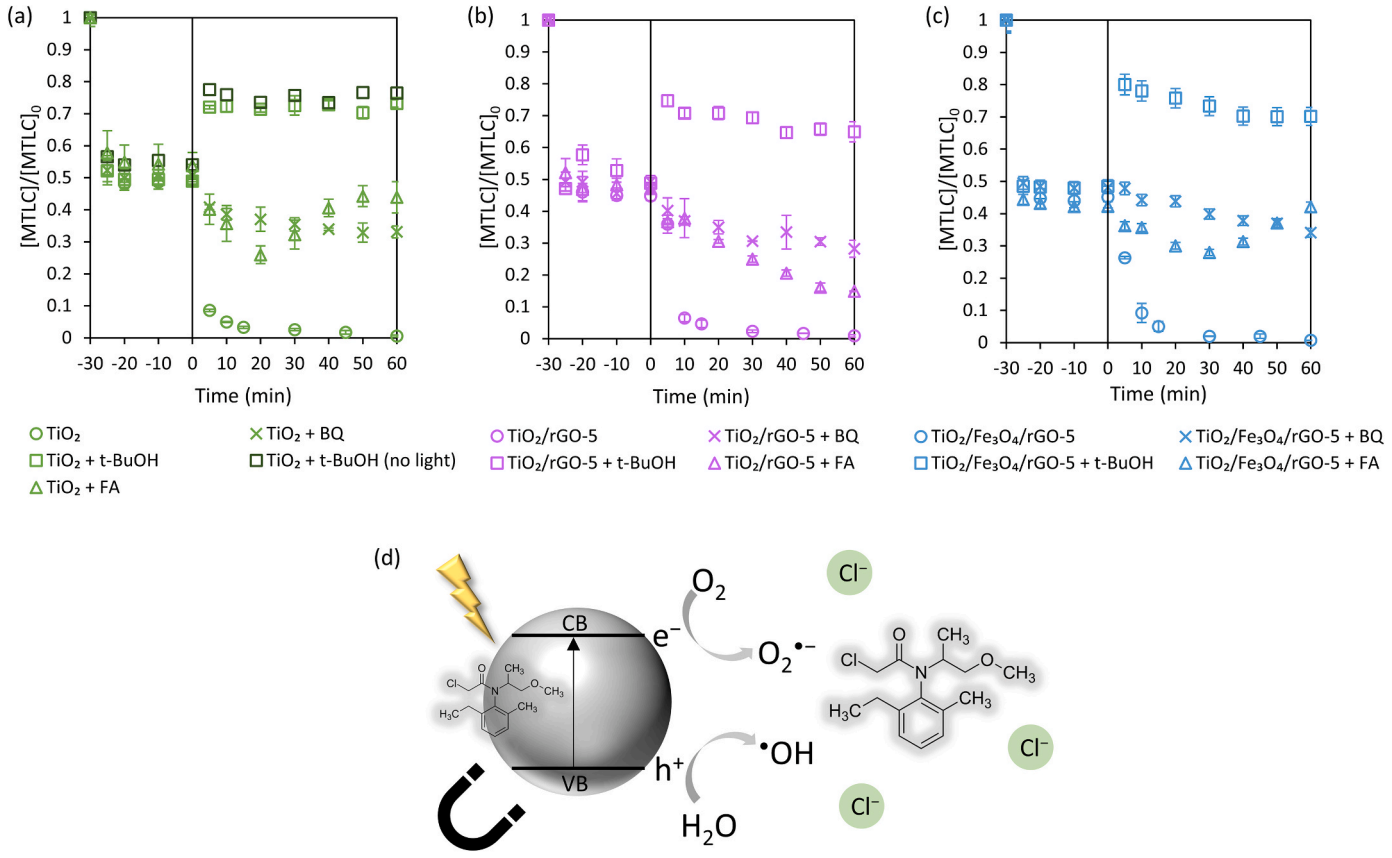

Fig. 6. MTLC evolution in experiments with different scavengers. 30 mg L^{-1} of MTLC and 0.5 g L^{-1} of (a) TiO_2, (b) TiO_2/rGO-5 and (c) TiO_2/Fe_3O_4/rGO-5. (d) Proposed graphical mechanism for TiO_2/Fe_3O_4/rGO-5.

TiO_2/Fe_3O_4/rGO-5, the presence of rGO accentuates the materials conductivity promoting the activity of superoxide radicals. Although the MTLC degradation patterns were quite similar for the three photocatalysts, the obtained results confirm that role of ROS are catalyst-dependent. The adsorption and photocatalytic properties of TiO_2/Fe_3O_4/rGO-5 show great promise for practical environmental applications.

Author contributions

Carmen Barquín: Conceptualization, Methodology, Validation, Investigation, Writing – original draft, Writing – review & editing, **María J. Rivero:** Conceptualization, Methodology, Validation, Writing – review & editing, Supervision, Resources, Project administration, Funding acquisition, **Inmaculada Ortiz:** Conceptualization, Methodology, Validation, Writing – review & editing, Supervision, Resources, Project administration, Funding acquisition.

Declaration of competing interest

The authors declare that they have no known competing financial interests or personal relationships that could have appeared to influence the work reported in this paper.

Data availability

The data that has been used is confidential.

Acknowledgements

These results are part of the R&D projects RTI2018-099407-B-I00 and RTI2018-093310-B-I00, funded by MCIN/AEI/10.13039/501100011033 and "ERDF A way of making Europe". Carmen Barquín is also grateful for the FPI contract PRE2019-089096.

Appendix A. Supplementary data

Supplementary data to this article can be found online at https://doi.org/10.1016/j.chemosphere.2022.135991.

References

Al-Mamun, M.R., Kader, S., Islam, M.S., Khan, M.Z.H., 2019. Photocatalytic activity improvement and application of UV-TiO_2 photocatalysis in textile wastewater treatment: a review. J. Environ. Chem. Eng. 7, 103248–103264. https://doi.org/10.1016/j.jece.2019.103248.

Balsamo, S.A., Fiorenza, R., Condorelli, M., Pecoraro, R., Brundo, M.V., Lo Presti, F., Sciré, S., 2021. Degradation of groundwater pollutants. Materials 14, 5938–5956. https://doi.org/10.3390/ma14205938.

Benjwal, P., Kumar, M., Chamoli, P., Kar, K.K., 2015. Enhanced photocatalytic degradation of methylene blue and adsorption of arsenic(III) by reduced graphene oxide (rGO)-metal oxide (TiO_2/Fe_3O_4) based nanocomposites. RSC Adv. 5, 73249–73260. https://doi.org/10.1039/c5ra13689j.

Bhatkhande, D.S., Pangarkar, V.G., Beenackers, A.A.C.M., 2002. Photocatalytic degradation for environmental applications - a review. J. Chem. Technol. Biotechnol. 77, 102–116. https://doi.org/10.1002/jctb.532.

Bibi, S., Ahmad, A., Anjum, M.A.R., Haleem, A., Siddiq, M., Shah, S.S., Kahtani, A.A., 2021. Photocatalytic degradation of malachite green and methylene blue over reduced graphene oxide (rGO) based metal oxides (rGO-Fe_3O_4/TiO_2) nanocomposite under UV-visible light irradiation. J. Environ. Chem. Eng. 9, 105580–105590. https://doi.org/10.1016/j.jece.2021.105580.

Boruah, P.K., Das, M.R., 2020. Dual responsive magnetic Fe_3O_4-TiO_2/graphene nanocomposite as an artificial nanozyme for the colorimetric detection and photodegradation of pesticide in an aqueous medium. J. Hazard Mater. 385, 121516–121532. https://doi.org/10.1016/j.jhazmat.2019.121516.

Cavalcante, R.P., Dantas, R.F., Bayarri, B., González, O., Giménez, J., Esplugas, S., Machulek Junior, A., 2016. Photocatalytic mechanism of metoprolol oxidation by photocatalysts TiO_2 and TiO_2 doped with 5% B: primary active species and intermediates. Appl. Catal. B Environ. 194, 111–122. https://doi.org/10.1016/j.apcatb.2016.04.054.

Chen, D., Cheng, Y., Zhou, N., Chen, P., Wang, Y., Li, K., Huo, S., Cheng, P., Peng, P., Zhang, R., Wang, L., Liu, H., Liu, Y., Ruan, R., 2020. Photocatalytic degradation of organic pollutants using TiO_2-based photocatalysts: a review. J. Clean. Prod. 268, 121725–121738. https://doi.org/10.1016/j.jclepro.2020.121725.

Cheng, L., Zhang, S., Wang, Y., Ding, G., Jiao, Z., 2016. Ternary P25-graphene-Fe_3O_4 nanocomposite as a magnetically recyclable hybrid for photodegradation of dyes. Mater. Res. Bull. 73, 77–83. https://doi.org/10.1016/j.materresbull.2015.06.047.

Corredor, J., Harankahage, D., Gloaguen, F., Rivero, M.J., Zamkov, M., Ortiz, I., 2021. Influence of QD photosensitizers in the photocatalytic production of hydrogen with biomimetic [FeFe]-hydrogenase. Comparative performance of CdSe and CdTe. Chemosphere 278, 130485–130493. https://doi.org/10.1016/j.chemosphere.2021.130485.

Corredor, J., Pérez-Peña, E., Rivero, M.J., Ortiz, I., 2020. Performance of rGO/TiO_2 photocatalytic membranes for hydrogen production. Membranes 10, 218–230. https://doi.org/10.3390/membranes10090218.

Diban, N., Pacuła, A., Kumakiri, I., Barquín, C., Rivero, M.J., Urtiaga, A., Ortiz, I., 2021. TiO_2–zeolite metal composites for photocatalytic degradation of organic pollutants in water. Catalysts 11, 1367–1378. https://doi.org/10.3390/catal11111367.

Fan, H., Yi, G., Zhang, X., Xing, B., Zhang, C., Chen, L., Zhang, Y., 2021. Facile synthesis of uniformly loaded Fe_3O_4–TiO_2/RGO ternary hybrids for enhanced photocatalytic activities. Opt. Mater. 111, 110582–110591. https://doi.org/10.1016/j.optmat.2020.110582.

Fernández-Castro, P., Vallejo, M., San Román, M.F., Ortiz, I., 2015. Insight on the fundamentals of advanced oxidation processes: role and review of the determination methods of reactive oxygen species. J. Chem. Technol. Biotechnol. 90, 796–820. https://doi.org/10.1002/jctb.4634.

Fogaça, L.Z., Vicentini, J.C.M., de Freitas, C.F., de Souza, M., Baesso, M.L., Caetano, W., Batistela, V.R., Olsen Scaliante, M.H.N., 2021. Reduced graphene oxide impregnated in TiO_2 for photodegradation of dyes monitored in UV-LED mini-reactor. Mater. Chem. Phys. 272, 125020–125028. https://doi.org/10.1016/j.matchemphys.2021.125020.

Fujishima, A., Zhang, X., Tryk, D.A., 2008. TiO_2 photocatalysis and related surface phenomena. Surf. Sci. Rep. 63, 515–582. https://doi.org/10.1016/j.surfrep.2008.10.001.

Gholami, P., Khataee, A., Soltani, R.D.C., Dinpazhoh, L., Bhatnagar, A., 2020. Photocatalytic degradation of gemifloxacin antibiotic using Zn-Co-LDH@biochar nanocomposite. J. Hazard Mater. 382, 121070–121081. https://doi.org/10.1016/j.jhazmat.2019.121070.

Gupta, B., Melvin, A.A., 2017. TiO_2/RGO composites: its achievement and factors involved in hydrogen production. Renew. Sustain. Energy Rev. 76, 1384–1392. https://doi.org/10.1016/j.rser.2017.03.123.

Hotloś, H., 2008. Quantity and availability of freshwater resources: the world – Europe – Poland. Environ. Protect. Eng. 34, 67–77.

Karimi-Maleh, H., Shafieizadeh, M., Taher, M.A., Opoku, F., Kiarii, E.M., Govender, P.P., Ranjbari, S., Rezapour, M., Orooji, Y., 2020. The role of magnetite/graphene oxide nano-composite as a high-efficiency adsorbent for removal of phenazopyridine residues from water samples, an experimental/theoretical investigation. J. Mol. Liq. 298, 112040–112048. https://doi.org/10.1016/j.molliq.2019.112040.

Karthikeyan, C., Arunachalam, P., Ramachandran, K., Al-Mayouf, A.M., Karuppuchamy, S., 2020. Recent advances in semiconductor metal oxides with enhanced methods for solar photocatalytic applications. J. Alloys Compd. 828, 154281–154295. https://doi.org/10.1016/j.jallcom.2020.154281.

Klein, C., Schneider, R.J., Meyer, M.T., Aga, D.S., 2006. Enantiomeric separation of metolachlor and its metabolites using LC-MS and CZE. Chemosphere 62, 1591–1599. https://doi.org/10.1016/j.chemosphere.2005.06.048.

Koe, W.S., Lee, J.W., Chong, W.C., 2020. An overview of photocatalytic degradation: photocatalysts, mechanisms, and development of photocatalytic membrane. J. Colloid Interface Sci. 27, 2522–2565. https://doi.org/10.1007/s11356-019-07193-5.

Li, X., Li, J., Bai, J., Dong, Y., Li, L., Zhou, B., 2016. The inhibition effect of tert-butyl alcohol on the TiO_2 nano assays photoelectrocatalytic degradation of different organics and its mechanism. Nano-Micro Lett. 8, 221–231. https://doi.org/10.1007/s40820-015-0080-2.

Li, Z.Q., Wang, H.L., Zi, L.Y., Zhang, J.J., Zhang, Y.S., 2015. Preparation and photocatalytic performance of magnetic TiO_2–Fe_3O_4/graphene (RGO) composites under VIS-light irradiation. Ceram. Int. 41, 10634–10643. https://doi.org/10.1016/j.ceramint.2015.04.163.

Liu, G., Feng, M., Tayyab, M., Gong, J., Zhang, M., Yang, M., Lin, K., 2021a. Direct and efficient reduction of perfluorooctanoic acid using bimetallic catalyst supported on carbon. J. Hazard Mater. 412, 125224–125234. https://doi.org/10.1016/j.jhazmat.2021.125224.

Liu, Y., Zhu, Q., Tayyab, M., Zhou, L., Lei, J., Zhang, J., 2021b. Single-atom Pt loaded zinc vacancies ZnO-ZnS induced type-V electron transport for efficiency photocatalytic H_2 evolution. Sol. RRL 5, 2100536–2100545. https://doi.org/10.1002/solr.202100536.

Ma, J., Graham, N.J.D., 2000. Degradation of atrazine by manganese-catalysed ozonation - influence of radical scavengers. Water Res. 34, 3822–3828. https://doi.org/10.1016/S0043-1354(00)00130-5.

Maimaiti, T., Hu, R., Yuan, H., Liang, C., Liu, F., Li, Q., Lan, S., Yu, B., Yang, S.T., 2022. Magnetic Fe_3O_4/TiO_2/graphene sponge for the adsorption of methylene blue in aqueous solution. Diam. Relat. Mater. 123, 108811–108817. https://doi.org/10.1016/j.diamond.2021.108811.

Minitha, C.R., Arachy, M.M.S., Kumar, R.T.R., 2018. Influence of Fe_3O_4 nanoparticles decoration on dye adsorption and magnetic separation properties of Fe_3O_4/rGO nanocomposites. Separ. Sci. Technol. 53, 2159–2169. https://doi.org/10.1080/01496395.2018.1446986.

Nguyen, C.H., Tran, M.L., van Tran, T.T., Juang, R.S., 2020. Enhanced removal of various dyes from aqueous solutions by UV and simulated solar photocatalysis over TiO_2/

ZnO/rGO composites. Separ. Purif. Technol. 232, 115962–115975. https://doi.org/10.1016/j.seppur.2019.115962.
Nosaka, Y., Nosaka, A.Y., 2017. Generation and detection of reactive oxygen species in photocatalysis. Chem. Rev. 117, 11302–11336. https://doi.org/10.1021/acs.chemrev.7b00161.
Oppenländer, T., 2002. Properties, reactivity and photochemistry of auxiliary chemicals. In: Photochemical Purification of Water and Air. Wiley Online Library, pp. 145–187. https://doi.org/10.1002/9783527610884.ch6.
Orge, C.A., Pereira, M.F.R., Faria, J.L., 2017. Photocatalytic-assisted ozone degradation of metolachlor aqueous solution. Chem. Eng. J. 318, 247–253. https://doi.org/10.1016/j.cej.2016.06.136.
Padmanabhan, N.T., Thomas, N., Louis, J., Mathew, D.T., Ganguly, P., John, H., Pillai, S. C., 2021. Graphene coupled TiO_2 photocatalysts for environmental applications: a review. Chemosphere 271, 129506–129538. https://doi.org/10.1016/j.chemosphere.2020.129506.
Pelaez, M., Falaras, P., Likodimos, V., O'Shea, K., de la Cruz, A.A., Dunlop, P.S.M., Byrne, J.A., Dionysiou, D.D., 2016. Use of selected scavengers for the determination of NF-TiO_2 reactive oxygen species during the degradation of microcystin-LR under visible light irradiation. J. Mol. Catal. Chem. 425, 183–189. https://doi.org/10.1016/j.molcata.2016.09.035.
Qin, Y., Mingce, L., Beihui, T., Baoxue, Z., 2014. RhB adsorption performance of magnetic adsorbent Fe_3O_4/RGO composite and its regeneration through A fenton-like reaction. Nano-Micro Lett. 6, 125–135. https://doi.org/10.5101/nml.v6i2.p125-135.
Ribao, P., Corredor, J., Rivero, M.J., Ortiz, I., 2019. Role of reactive oxygen species on the activity of noble metal-doped TiO_2 photocatalysts. J. Hazard Mater. 372, 45–51. https://doi.org/10.1016/j.jhazmat.2018.05.026.
Rodríguez, E.M., Márquez, G., Tena, M., Álvarez, P.M., Beltrán, F.J., 2015. Environmental Determination of main species involved in the first steps of TiO_2 photocatalytic degradation of organics with the use of scavengers : the case of ofloxacin. Appl. Catal. B Environ. 178, 44–53. https://doi.org/10.1016/j.apcatb.2014.11.002.
Sakkas, V.A., Arabatzis, I.M., Konstantinou, I.K., Dimou, A.D., Albanis, T.A., Falaras, P., 2004. Metolachlor photocatalytic degradation using TiO_2 photocatalysts. Appl. Catal. B Environ. 49, 195–205. https://doi.org/10.1016/j.apcatb.2003.12.008.
Schuchmann, M.N., Bothe, E., von Sonntag, J., von Sonntag, C., 1998. Reaction of OH radicals with benzoquinone in aqueous solutions. A pulse radiolysis study. J. Chem. Soc.-Perkin Trans. 2, 791–796.
Sun, H., Cao, L., Lu, L., 2011. Magnetite/reduced graphene oxide nanocomposites: one step solvothermal synthesis and use as a novel platform for removal of dye pollutants. Nano Res. 4, 550–562. https://doi.org/10.1007/s12274-011-0111-3.
Tayyab, M., Liu, Y., Min, S., Irfan, R.M., Zhu, Q., Zhou, L., Lei, J., Zhang, J., 2022. Simultaneous hydrogen production with the selective oxidation of benzyl alcohol to benzaldehyde by a noble-metal-free photocatalyst VC/CdS nanowires. Chin. J. Catal. 43, 1165–1175. https://doi.org/10.1016/S1872-2067(21)63997-9.
USEPA, 2022. Drinking water contaminant candidate list (CCL) and regulatory determination. https://www.epa.gov/ccl.
Varma, K.S., Tayade, R.J., Shah, K.J., Joshi, P.A., Shukla, A.D., Gandhi, V.G., 2020. Photocatalytic degradation of pharmaceutical and pesticide compounds (PPCs) using doped TiO_2 nanomaterials: a review. Water-Energy Nexus 3, 46–61. https://doi.org/10.1016/j.wen.2020.03.008.
Vieira Guelfi, D.R., Gozzi, F., Machulek, A., Sirés, I., Brillas, E., de Oliveira, S.C., 2018. Degradation of herbicide S-metolachlor by electrochemical AOPs using a boron-doped diamond anode. Catal. Today 313, 182–188. https://doi.org/10.1016/j.cattod.2017.10.026.
Vital-Grappin, A.D., Ariza-Tarazona, M.C., Luna-Hernández, V.M., Villarreal-Chiu, J.F., Hernández-López, J.M., Siligardi, C., Cedillo-González, E.I., 2021. The role of the reactive species involved in the photocatalytic degradation of HDPE microplastics using C,N-TiO_2 powders. Polymers 13, 999–1016. https://doi.org/10.3390/polym13070999.
Wanag, A., Kusiak-Nejman, E., Czyżewski, A., Moszyński, D., Morawski, A.W., 2021. Influence of rGO and preparation method on the physicochemical and photocatalytic properties of TiO_2/reduced graphene oxide photocatalysts. Catalysts 11, 1133–1352. https://doi.org/10.3390/catal11111333.
Wang, J., Zhang, Q., Deng, F., Luo, X., Dionysiou, D.D., 2020. Rapid toxicity elimination of organic pollutants by the photocatalysis of environment-friendly and magnetically recoverable step-scheme $SnFe_2O_4$/$ZnFe_2O_4$ nano-heterojunctions. Chem. Eng. J. 379, 122264–122274. https://doi.org/10.1016/j.cej.2019.122264.
Zemolin, C.R., Avila, L.A., Cassol, G.V., Massey, J.H., Camargo, E.R., 2014. Environmental fate of S-metolachlor - a review -. Planta Daninha 32, 655–664. https://doi.org/10.1590/S0100-83582014000300022.
Zhou, S., Jin, M., Tan, R., Shen, Z., Yin, J., Qiu, Z., Chen, Z., Shi, D., Li, H., Yang, Z., Wang, H., Gao, Z., Li, J., Yang, D., 2022. A reduced graphene oxide-Fe_3O_4 composite functionalized with cetyltrimethylammonium bromide for efficient adsorption of SARS-CoV-2 spike pseudovirus and human enteric viruses. Chemosphere 291, 132995–133006. https://doi.org/10.1016/j.chemosphere.2021.132995.